PAPER

Facile preparation of Ag/Ni(OH)$_2$ composites with enhanced catalytic activity for reduction of 4-nitrophenol†

Feng Bao, Fatang Tan,* Wei Wang, Xueliang Qiao and Jianguo Chen

In this work, a facile and environmentally friendly process was developed for synthesis of Ag/Ni(OH)$_2$ composites by only mixing an ethanol solution of AgNO$_3$ with Ni(OH)$_2$ at room temperature. The morphology and structure of the as-prepared Ag/Ni(OH)$_2$ composites were investigated by X-ray diffraction (XRD), field-emission scanning electron microscopy (FESEM), transmission electron microscopy (TEM), high resolution TEM (HRTEM) and X-ray photoelectron spectroscopy (XPS). It was found that the composites consist of ultrathin nickel hydroxide and silver nanoparticles (Ag NPs), the Ag NPs with an average diameter of around 4.7 nm evenly dispersed on the surface of Ni(OH)$_2$ nanosheets. The catalytic properties of the obtained Ag/Ni(OH)$_2$ composites were evaluated by the reduction of 4-nitrophenol (4-NP) using NaBH$_4$ as a reducing agent. The results revealed that the obtained Ag/Ni(OH)$_2$ composites exhibited an outstanding catalytic activity. In addition, the formation mechanism of Ag NPs was probed by ultraviolet-visible spectroscopy (UV-Vis). It was found that Ni(OH)$_2$ as a substrate played an important role in the formation of silver particles, which not only acted as a superior adsorbent of silver ion but also a source of OH$^-$ that was able to accelerate the reaction. Electrochemical impedance spectroscopy (EIS) and fluorescence (FL) spectra were employed to indirectly elucidate the mechanism for reduction of 4-NP. The Ag/Ni(OH)$_2$ composites are very promising catalytic candidates for the reduction of 4-nitrophenol because of their easy and simple preparation route and high catalytic activity.

1. Introduction

Noble metal nanoparticles (Ag, Au, Pt, *etc.*) have been used in many fields including electronics, energy, biotechnology and catalysis.[1–5] Ag NPs have been of great interest during the past decades because of their relatively inexpensive price and excellent catalytic performance. Many reactions are catalyzed by Ag NPs, whose properties are largely influenced by the size, shape, and dispersion. In general, smaller particles more easily aggregate due to their greater surface area and higher surface energy, which will prevent them from large scale use.[6] So it is common that some dispersants or protective agents are employed to inhibit the aggregation of nanoparticles during the preparation process. On the other hand, organic modifiers would cap around the particles surface of catalysts and interact with them, which will consequently lead to a distinct decrease of catalytic activities.[7] Therefore, some improvements have already been taken to solve the problem. One of applicable strategies is to deposit Ag NPs on different supports to form various composites, such as Ag/carbon materials, Ag/metallic oxide, Ag/nonmetallic oxide and Ag/metal hydroxide, which have been successfully synthesized and attracted extensive attention due to their superior performance as catalysts.[8–11]

Nickel hydroxide (Ni(OH)$_2$), one of the most important transition metal hydroxides, has been intensively studied and widely used in storage batteries, electroplating and catalyst support.[12–14] Numerous methods like hydrothermal and solvothermal methods, precipitation, sol–gel method have been employed for synthesis of Ni(OH)$_2$ with various shapes, such as nanosheets, nanoparticles, nanoribbons, nanospheres, *etc.*[15] Zhen *et al.* had fabricated Pd$_x$-Pt$_{1-x}$/Ni(OH)$_2$ hybrids by mixing L-arginine modified Ni(OH)$_2$ nanosheets and PVP stabilized Pd$_x$Pt$_{1-x}$ nanoparticles for the reduction of 4-NP.[16] And Chen *et al.* had synthesized three-dimensional (3D) Ag/β-Ni(OH)$_2$ flower microspheres through a hydrothermal method in the presence of L-arginine.[17] As catalyst, Ni(OH)$_2$ was used for hydrogen production and degradation of dyes.[18,19] What is more, Ni(OH)$_2$ has large surface areas and showed excellent synergistic effects with other catalytically active components according to previous reports.[16] So it may be suitable for loading noble metal nanoparticles for the aforementioned reasons. To the best of our knowledge, the use of Ni(OH)$_2$ for both as a adsorbent and a support has been rarely studied.

In this paper, we reported the successful synthesis of Ag/Ni(OH)$_2$ composites *via* a very simple and convenient autocatalytic

State Key Laboratory of Materials Processing and Die & Mould Technology, Huazhong University of Science and Technology, Wuhan, 430074, Hubei, PR China. E-mail: Fatangtan@hust.edu.cn; Fax: +86 27 87541540; Tel: +86 27 87541540

† Electronic supplementary information (ESI) available. See DOI: 10.1039/c6ra27153g

reduction method in ethanol system. $Ni(OH)_2$ nanosheets introduced as carrier and adsorbent were prepared by chemical precipitation method. $Ag/Ni(OH)_2$ composites were prepared by mixing ethanol solution of $AgNO_3$ and $Ni(OH)_2$ under magnetic stirring at room temperature, without addition of any strong reductant or surfactant. The catalytic properties of the obtained $Ag/Ni(OH)_2$ composites were investigated by employing the reduction of 4-NP to 4-AP by $NaBH_4$ as a model reaction and the $Ag/Ni(OH)_2$ composites showed excellent catalytic activity. And the formation mechanism of the obtained $Ag/Ni(OH)_2$ composites was discussed by several groups of comparative experiments.

2. Experimental

2.1 Materials

All the reagents used in this work were analytical grade and used without further purification or treatment. Nickel nitrate $(Ni(NO_3)_2 \cdot 6H_2O)$, potassium hydroxide (KOH), silver nitrate $(AgNO_3; 99.8\%)$, anhydrous ethanol, sodium borohydride $(NaBH_4)$ and 4-nitrophenol $(4\text{-}C_6H_5NO_3)$ were all purchased from Sinopharm Chemical Reagent Co., Ltd (Shanghai, China). Double-distilled water was used in all of the experiments.

2.2 Preparation of $Ni(OH)_2$ nanosheets

The preparation of $Ni(OH)_2$ nanosheets was performed by chemical precipitation method. Typically, 1 mmol $Ni(NO_3)_2 \cdot 6H_2O$ was dissolved in 20 mL deionized water $(0.05\ mol\ L^{-1})$ and then 50 mL solution containing 0.142 g KOH was dropped at a certain speed. After that the mixture was stirred for 2 h to get a greenish paste like precipitate. The precipitate was allowed to settle for 12 h. Finally, the sample was washed with deionized water for three times and anhydrous ethanol for two times by repeated centrifugation until the precipitate was free from alkali. The precipitate was then redispersed in 20 mL anhydrous ethanol for later use.

2.3 Synthesis of $Ag/Ni(OH)_2$ composites

0.095 g $AgNO_3$ was dissolved in 50 mL anhydrous ethanol by ultrasound. A certain volume of $AgNO_3$ ethanol solution with the concentration of 1.9 g L^{-1} was added to above $Ni(OH)_2$ ethanol solution to prepare $Ag/Ni(OH)_2$ composites with various theoretical Ag loadings (2, 5, 7, 10, 12, 15 wt%). The resulting suspension was stirred for 2 h and the solution color changed from light green to dark-brown (Fig. S1†). And the higher volume of silver nitrate ethanol solution was added, the darker the color of the solution was. At last the suspensions were treated with high-speed centrifugation to separate the composites out from ethanol solution and dried in a vacuum oven at 35 °C for 12 h (Fig. S2†). The products are denoted as $Ag(x)/Ni(OH)_2$, where x represents theoretical Ag content (wt%) in the $Ag/Ni(OH)_2$ composites.

2.4 Characterization

Powder X-ray diffraction (XRD) patterns were obtained on a Philips X'Pert PRO diffractometer (Cu K_α, $\lambda = 1.5406$ Å) with an accelerating voltage of 40 kV and applied current of 40 mA. UV-Vis spectrum was recorded using a UV-2550 spectrophotometer (Shimadzu Co., Japan). The morphology and the size of the composites were collected on a field emission scanning electron microscope (FESEM, Sirion 450, FEI Company, Holland) equipped with an X-ray energy dispersive spectrometer (EDS) at 20 kV. And the Ag nanoparticles were investigated with an H-7000FA transmission electron microscope (Hitachi) at an operating voltage of 75 kV. The XPS measurements were performed on a Kratos/Axis Ultra DLD-600W spectrometer with Mg Kα source. The contents of silver element in the composites were detected by an atomic absorption spectroscopy (AAS) model iCE 3000 series (Thermo Scientific). The samples were prepared by nitrating a certain amount of the composites and then diluted to a certain concentration. Fourier transform infrared (FT-IR) were obtained using a FTIR spectrometer (Bruker VERTEX70). The room temperature fluorescence (FL) spectra were recorded on a fluorescence spectrometer (RF-5301 PC, Japan) with excitation wavelength of 325 nm.

2.5 Catalytic reduction of 4-NP

The catalytic activities of the synthesized $Ag/Ni(OH)_2$ composites were evaluated by the reduction of 4-NP to 4-AP using $NaBH_4$ as reducing agent at 25 °C. In a typical run, 3.3 mL of freshly prepared aqueous solution of $NaBH_4$ (0.3 M) was introduced to 100 mL of 4-NP (0.1 mM) solution. The color of the solution turned from light yellow to deep yellow immediately, and then 4 mg of the $Ag/Ni(OH)_2$ composites were added. About 3 mL of the mixture was filtered through a 0.45 μm membrane filter every 2 minutes and measured with UV-Vis absorption spectra in the range from 250 nm to 500 nm.

2.6 Electrochemical measurement

Electrochemical impedance spectroscopy (EIS) measurements were tested using a CS350 electrochemical analyser (CorrTest, China) with a single-compartment three-electrode glass cell. The impedance spectra of the electrodes were recorded from 10 kHz to 10 mHz with an AC voltage magnitude of 10 mV. Platinum foil and a saturated calomel electrode were used as a counter electrode and a reference electrode, respectively. As-prepared sample was used as working electrode. The working electrode was prepared by mixing 0.05 g catalyst with 0.125 mL water and 0.02 g polyethylene glycol (PEG, molecular weight: 20 000) and ground to obtain a slurry. Then the slurry was coated on a FTO glass (2 cm × 1.5 cm) by doctor-blade method. Finally, the glass electrode was calcined at 180 °C for 0.5 h. 0.1 M Na_2SO_4 solution was used as the electrolyte solution. All the measurements were carried out at room temperature.

3. Results and discussion

3.1 Synthesis and characterization of $Ag/Ni(OH)_2$ composites

The overall crystallinity and crystal structures of the synthesized samples were examined by X-ray diffraction (XRD). Fig. 1 shows XRD patterns of the obtained $Ni(OH)_2$ nanosheets and the as-prepared $Ag/Ni(OH)_2$ composites with different Ag contents. The broad diffraction peaks of the samples $Ni(OH)_2$ and Ag/
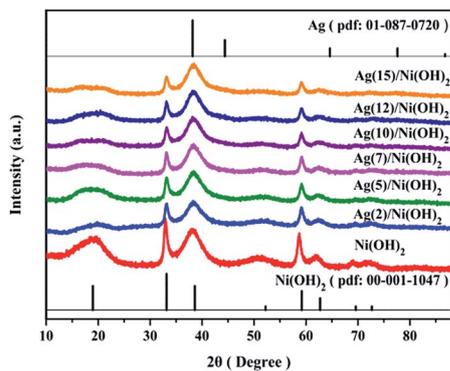
Paper

Fig. 1 XRD patterns of the Ni(OH)$_2$ and Ag/Ni(OH)$_2$ composites.

Ni(OH)$_2$ suggest that the crystallite sizes are very small.[20] Diffraction peaks of Ni(OH)$_2$ observed at 2θ values of 19.0°, 33.2°, 38.6°, 51.8°, 59.2°, 62.7°, 69.6°and 72.7° match well with the hexagonal Ni(OH)$_2$ phase (JCPDS 01-1047, 0117), and no peaks from other phases are detected. The diffraction peak at 2θ value of 33.2° is the strongest peak. But it can be observed that the diffraction intensity of the peak at 33.2° becomes weaker with the increase of Ag content for Ag/Ni(OH)$_2$ composites. And the strongest peak of the Ag/Ni(OH)$_2$ composites changed from 33.2° to 38.6°. Although no distinct diffraction peaks of Ag were observed, which may be due to the low content and high dispersion of Ag NPs in the composites, the strongest peak of the composites at 38.6° was in a similar position to the strongest peak of the silver at 38.2° as shown in Fig. 1. According to the variation of the intensity of the peaks, we may be able to conclude the formation of Ag NPs.

UV-Vis spectra of the as-prepared Ag/Ni(OH)$_2$ composite solutions and Ni(OH)$_2$ suspensions is shown in Fig. 2. The absorption peak at about 409 nm is the characteristic peak of Ag NPs, indicating the generation of Ag NPs in the solution. During the synthesis, the silver ions were reduced to form silver nanoparticles which dispersed on Ni(OH)$_2$ nanosheets and the solution color changed from light green to dark brown. The whole preparation procedure of Ag(x)/Ni(OH)$_2$ composites is monitored by recording the absorption spectra of the reaction solution as a function of Ag
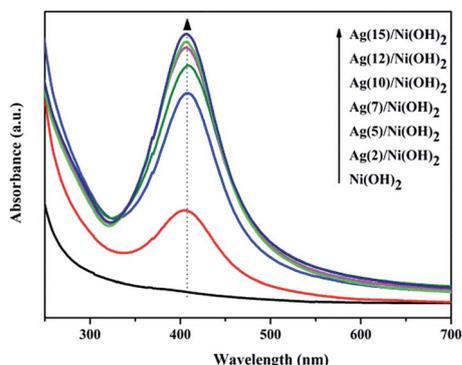
contents. With the increase of Ag contents, the absorbance increased, indicating the continuous deposition of Ag atoms on Ni(OH)$_2$ nanosheets. However, the growth rate gradually slowed down. In the end, the absorbance only has a small increase, which may be due to the limited active sites on the surface of Ni(OH)$_2$ nanosheets. The peak becomes narrower with a decreased band width and an increased band intensity with the increase of silver content in the composites, so we can conclude the size of Ag NPs increase according to an inverse linear relationship between the full-width at half-maximum (FWHM) and the diameter of particles (D).

$$FWHM = 50 + 230/D \text{ (ref. 21)}$$

The morphology and microstructure of the samples were observed by SEM and TEM (Fig. 3). As shown in Fig. 3a, SEM image shows that Ag(10)/Ni(OH)$_2$ composites with a wide size distribution of diameter ranging from tens of nanometers to several microns have irregular shapes. EDS spectrum (Fig. 3b)
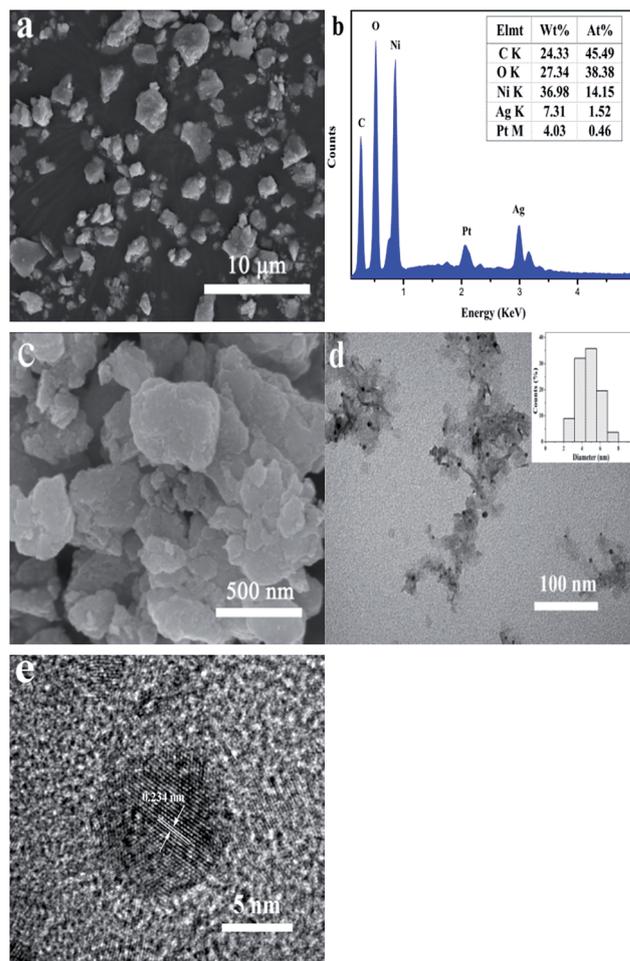

Fig. 3 (a) SEM images of the Ag(10)/Ni(OH)$_2$ composites with low magnification; (b) EDS spectrum of the Ag(10)/Ni(OH)$_2$ composites; (c) SEM images of the Ag(10)/Ni(OH)$_2$ composites with high magnification; (d) TEM images of the Ag(10)/Ni(OH)$_2$ composites and the corresponding size distribution of Ag NPs; (e) HRTEM image of the Ag(10)/Ni(OH)$_2$ composites.

Fig. 2 UV-Vis spectra of the as-prepared Ag/Ni(OH)$_2$ composite solutions.

exhibits the characteristic peaks of silver at *ca.* 3.0 keV, which also confirms the presence of Ag in the composites. High-magnification SEM image reveals that the composites are sheets-like structure and a large sheet is composed of a serials of smaller sheets (Fig. 3c), which were further confirmed by TEM image in Fig. 3d. And it can be clearly seen that Ag NPs with an average diameter of around 4.7 nm are evenly distributed on the surface of $Ni(OH)_2$ nanosheets. There are no scattered Ag NPs outside of $Ni(OH)_2$ nanosheets surface. The morphology of $Ni(OH)_2$ nanosheets without Ag NPs is similar to that of the composites (Fig. S3†). The surface chemistry homogeneity of $Ag/Ni(OH)_2$ composites were characterized by elemental mapping technology, shown in Fig. S4.† It can be seen that related elemental mapping of Ni, Ag, and O are well distributed. Particularly, the element mapping of Ag indicates that Ag NPs are uniformly distributed on $Ni(OH)_2$ nanosheets. Furthermore, the HRTEM image shown in Fig. 3e suggests that the $Ni(OH)_2$ nanosheets may consist of even smaller nanocrystallites and the attached silver nanoparticle has a lattice distance of 0.234 nm (as marked), corresponding to the (111) crystal plane of metallic silver.[16,22]

In order to further confirm the deposition of Ag NPs on $Ni(OH)_2$ nanosheets surfaces, XPS characterization was performed in the region of 0–1200 eV (Fig. 4). The wide scan spectrum in Fig. 4a reveals the existence of oxygen, silver and nickel elements, which is in good agreement with the EDS analysis. Fig. 4b shows the high resolution XPS spectrum of Ag 3d. There are two peaks at 368.3 eV and 374.3 eV corresponding to the binding energies of Ag $3d_{5/2}$ and Ag $3d_{3/2}$, respectively, ascribed to the metal Ag. The value of Ag detected by the XPS was 6.44%, which is lower than the silver content measured by

AAS (8.37%). The reason is possible that only the elements located on the surface of composites can be detected by XPS survey. Fig. 4c shows the high resolution spectrum of Ni 2p, it is observed that two characteristic peaks of Ni $2p_{3/2}$ and Ni $2p_{1/2}$ are located at 855.4 and 873.1 eV, respectively, with a spin-energy separation of 17.7 eV, which is characteristic of the $Ni(OH)_2$ phase. The binding energy 855.4 eV is lower than previous reports (*ca.* 856 eV), indicating low valence of surface nickel, which may be because of the partial reduction of nickel ions.[23] In addition, some extra lines marked as satellite peaks (879.2 eV, 861.4 eV) around the Ni $2p_{1/2}$ and Ni $2p_{3/2}$ signals are also observed.

3.2 Catalytic activity for reduction of 4-nitrophenol

4-NP is a well-known toxic pollutant and the product (4-AP) is an important intermediate for the production of analgesic, antipyretic drugs, photographic developer, corrosion inhibitor, hair-dyeing agent and so on. The reduction of 4-NP to 4-AP by $NaBH_4$ was chosen as a model reaction to evaluate the catalytic properties of the as-prepared $Ag/Ni(OH)_2$ composites. Typically, the original absorption peak of 4-NP shifted from 317 nm to 400 nm due to the formation of 4-NP ions upon the addition of freshly prepared $NaBH_4$ solution.[24] When adding $Ni(OH)_2$ nanosheets, there was little decrease in the absorbance of nitro compound at 400 nm monitored by UV, suggesting the influence of adsorption could be ignored, $Ni(OH)_2$ nanosheets exhibited no hydrogenation activity (Fig. S5†). Whereas the absorption peak at 400 nm started to decrease when the reduction proceeded after the addition of $Ag/Ni(OH)_2$ composites (Fig. 5a). Since $NaBH_4$ was in large excess to 4-NP, its concentration could be considered as a constant during the reaction period. So the reduction rate can be evaluated by the pseudo-first-order kinetics with respect to 4-NP. Fig. 5b shows $\ln(C_t/C_0)$ *versus* reaction time t, apparently, they all display an almost linear evolution, slopes of which give the rate constants (k). $\ln[C_t/C_0] = kt$.

C_t and C_0 correspond to the concentrations of 4-NP at time t and 0, respectively.[25] $Ag(10)/Ni(OH)_2$ exhibited the highest catalytic activity, and the rate constant k is calculated to be 0.282 min^{-1}. Furthermore, the catalytic activity order of the
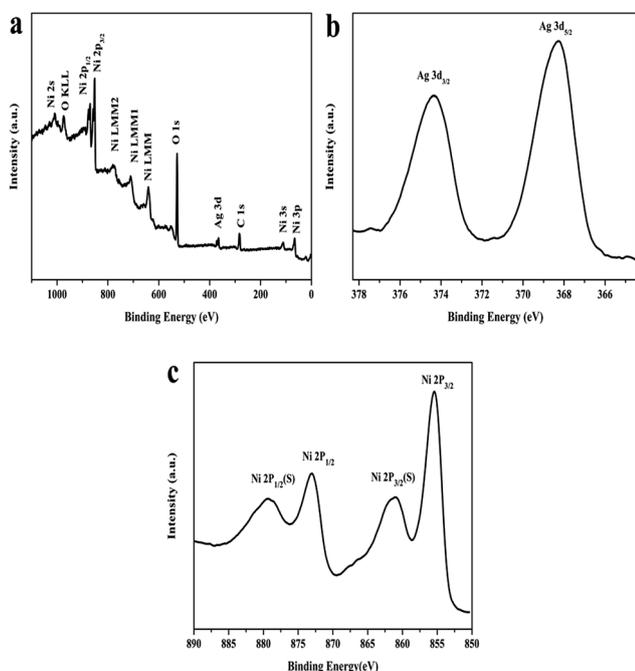

Fig. 4 (a) XPS spectra of $Ag(10)/Ni(OH)_2$; (b) high resolution spectrum of Ag 3d; (c) high resolution spectrum of Ni 2p.
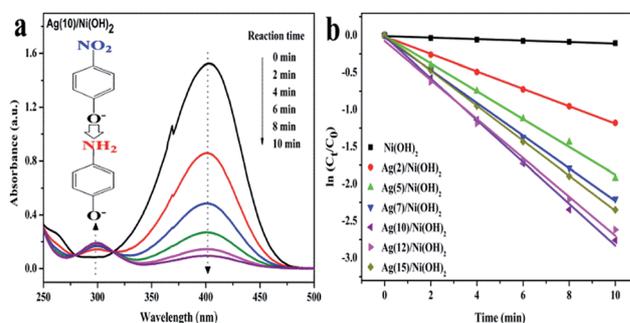

Fig. 5 (a) UV-Vis spectra of the 4-NP solution after adding $NaBH_4$ solution using $Ag(10)/Ni(OH)_2$ as a catalyst; (b) plots of $\ln(C_t/C_0)$ *versus* time for catalytic reduction of 4-NP using composites with different content of Ag NPs.

Table 1 The rate constants k and K' of different composites

Samples	k (min^{-1})	K' (min^{-1} g^{-1})	R^2
Ni(OH)$_2$	0.0099	2.4750	0.94655
Ag(2)/Ni(OH)$_2$	0.1173	29.325	0.99922
Ag(5)/Ni(OH)$_2$	0.1874	46.85	0.99651
Ag(7)/Ni(OH)$_2$	0.2202	55.05	0.99864
Ag(10)/Ni(OH)$_2$	0.2818	70.45	0.99728
Ag(12)/Ni(OH)$_2$	0.2623	65.58	0.99493
Ag(15)/Ni(OH)$_2$	0.2360	59	0.99985

catalysts was Ag(10)/Ni(OH)$_2$ > Ag(12)/Ni(OH)$_2$ > Ag(15)/Ni(OH)$_2$ > Ag(7)/Ni(OH)$_2$ > Ag(5)/Ni(OH)$_2$ > Ag(2)/Ni(OH)$_2$ > Ag(0)/Ni(OH)$_2$. The catalytic parameters for reduction of 4-nitrophenol are given in Table 1, K' is defined as the activity factor k over the weight of catalysts. Based on the weight of silver in the composites Ag(10)/Ni(OH)$_2$ (8.37%, measured by AAS), the activity factor k over the weight of silver is calculated to be 841.61 min^{-1} g^{-1}, which is much higher than that of Ag NPs deposited on the surface of micron silica spheres by the combination of surface functionalization deposition and seed-mediated growth technique (37.16 min^{-1} g^{-1}).[10]

We have also investigated the cyclic stability of sample Ag(10)/Ni(OH)$_2$ by monitoring the catalytic activity during successive cycles of the reduction reactions (Fig. 6). The procedure was the same at the beginning, about 3 mL of the mixture was taken after 10 min. After that, another 1 mL of the solution of 4-NP (10 mM) and 1 mL of the solution of NaBH$_4$ (0.3 M) were added for another cycle. The result showed that Ag(10)/Ni(OH)$_2$ composites maintain a high catalytic activity after five cycle times. Compared to fresh catalysts, some new peaks were found in the FTIR spectrum of used Ag(10)/Ni(OH)$_2$ after five cycles (Fig. S6†). The two weak peaks at 1465 cm^{-1} and 1449 cm^{-1} correspond to the skeletal vibration peak of benzene ring, and the peak located at 1272 cm^{-1} is ascribed to the stretching vibration of C–O from the radical cation intermediate (OHC$_6$H$_4$NH$_2$)$^+$.[26] The results indicate that a small amount of 4-AP may be adsorbed on the surface of catalysts. In addition, the morphology of the catalysts after five cycles has almost no
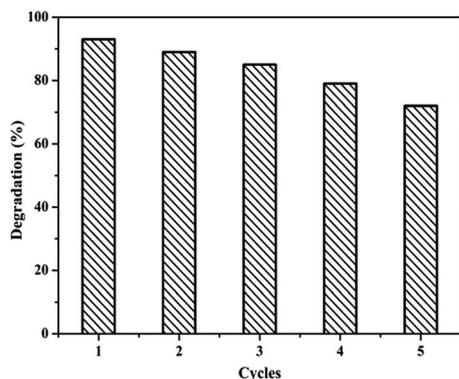
change (Fig. S7†), compared with that of the original sample (Fig. 3).

3.3 Mechanism for the formation of Ag/Ni(OH)$_2$ composites

To better understand the formation mechanism of the Ag/Ni(OH)$_2$, we carried out a batch of verification experiments under different conditions as shown in Fig. 7. Fig. 7a shows the UV-Vis absorbance spectra of the solutions under different conditions. The ethanol solution of Ni(OH)$_2$ and AgNO$_3$ was stirred at room temperature for two hours in condition a, then the other conditions, and so on. The color of the solution under the condition of b was darker than that of the solution under the condition of c, but the XRD patterns of the samples were similar as shown in Fig. 7b. And there is no absorption peaks of Ag NPs which indicated there is no formation of Ag NPs in the solution. What is more, the pH value changed from 6.97 to 7.60 under the condition of c, which indicated that Ni(OH)$_2$ could produce small amount of OH$^-$. From the above experimental results, we can conclude that the change of the solution color is due to the formation of Ag$_2$O on the surface of Ni(OH)$_2$ nanosheets. As for XRD patterns, it may be because of the low content and the nanocrystal nature of Ag$_2$O. It has been reported that ethanol could reduce silver ion to silver atom under heating condition.[27] For comparison, we stirred an ethanol silver nitrate solution (1.9 g L^{-1}) without Ni(OH)$_2$ nanosheets at room temperature for 2 h in condition d. The UV-Vis spectrum demonstrated that there is almost no reduction reaction occurred in pure ethanol. So the reduction of silver ions by ethanol at room temperature is negligible in the course of this experiment. However, when we mixed Ni(OH)$_2$ and 10 wt% AgNO$_3$ in the ethanol solution for 2 hours, the color of the solution changed from light green to dark-brown and the UV-Vis spectrum indicated the generation of Ag NPs in the solution clearly. So we can conclude the ethanol acted as reducing agent here. From what were mentioned above, Ni(OH)$_2$, AgNO$_3$ and ethanol are the three indispensable components for the synthesis of Ag/Ni(OH)$_2$ composites.
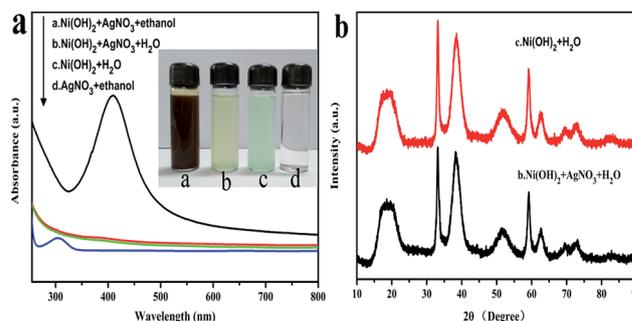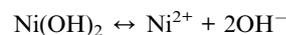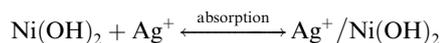
$$\mathrm{Ni(OH)}_2 + \mathrm{Ag}^+ \xleftrightarrow{\text{absorption}} \mathrm{Ag}^+/\mathrm{Ni(OH)}_2$$

$$\mathrm{Ni(OH)}_2 \leftrightarrow \mathrm{Ni}^{2+} + 2\mathrm{OH}^-$$

Fig. 6 The reusability of Ag(10)/Ni(OH)$_2$ as a catalyst for the reduction of 4-NP with NaBH$_4$.

Fig. 7 (a) UV-Vis absorbance spectra of the solutions under different conditions; (b) XRD patterns.

$$2Ag^+/Ni(OH)_2 + 2OH^- \leftrightarrow 2AgOH/Ni(OH)_2 \leftrightarrow$$
$$Ag_2O/Ni(OH)_2 + H_2O$$

$$CH_3CH_2OH + Ag_2O/Ni(OH)_2 \xrightarrow{OH^-}$$
$$2Ag/Ni(OH)_2 + H_2O + CH_3CHO$$

$$CH_3CHO + Ag_2O/Ni(OH)_2 + OH^- \rightarrow$$
$$CH_3COO^- + 2Ag/Ni(OH)_2 + 2Ag + H_2O$$
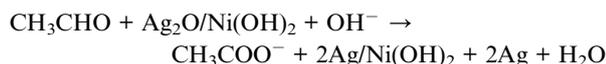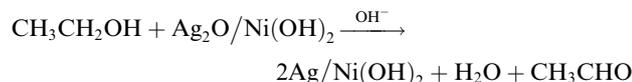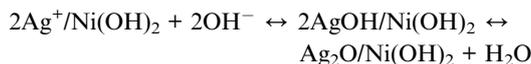
The above-described reaction is similar to the previous reported reaction of AgNO$_3$ and NaOH in ethanol system.[7] The possible reaction mechanism which has been proposed and demonstrated is that OH$^-$ and Ag$^+$ reacted to form Ag$_2$O particles firstly, then Ag$_2$O particles were reduced by ethanol molecules in the presence of hydroxide ions. Taking into account that the nickel hydroxide is a moderately strong bases and has excellent adsorption abilities to heavy metal ions.[13] The as-prepared Ni(OH)$_2$ was used to adsorb silver ions and it had a relatively large adsorption capacity of 37.5 mg g^{-1}. Therefore, we can conclude the formation mechanism of the Ag/Ni(OH)$_2$ composite is as follows. First, Ni(OH)$_2$ adsorbed silver ions to form Ag$_2$O particles. And then Ag$_2$O particles were reduced by ethanol molecules to form Ag atoms. So Ni(OH)$_2$ nanosheets is a carrier and an adsorbent here. To gain further insight into the detailed mechanism, however, more work is warranted.

3.4 Mechanism for reduction of 4-NP

The adsorption of 4-NP onto the catalyst and the electron transfer are both important factors in determining the catalytic performance for 4-NP reduction.[28] And it is known that the catalytic reduction of 4-NP to 4-AP is an electron transfer process.[29] So EIS was carried out to investigate the electron-transfer resistance of the catalyst to further study the reduction reaction of 4-NP to 4-AP. In Nyquist diagram, a smaller arc radius means a more facile charge transfer process at the interface of electrode.[30] As shown in Fig. 8a, the faradaic impedance spectra of pure Ni(OH)$_2$ and Ag(10)/Ni(OH)$_2$ are presented as Nyquist plots ($-Z''$ versus Z'). It can be seen that Ag(10)/Ni(OH)$_2$ composite shows faster interfacial charge transfer compared to the Ni(OH)$_2$, that means the presence of Ag NPs can promote the transfer of interfacial electron, which is beneficial for the reduction reaction of 4-NP to 4-AP.[31] Fluorescence spectra of pure Ni(OH)$_2$ and Ag(10)/Ni(OH)$_2$ are given in Fig. 8b. Compared with pure Ni(OH)$_2$, the emission intensity of Ag(10)/Ni(OH)$_2$ is drastically quenched after loading with Ag NPs due to the electron transfer from Ni(OH)$_2$ to Ag NPs, which indicates that Ag NPs are very efficient trap centres for charge transfer between nickel hydroxide and Ag NPs.[32,33] Therefore, Ag(10)/Ni(OH)$_2$ composite exhibits high catalytic activity.

According to the traditional theory about the catalytic reduction of 4-NP and the above experimental results, a catalytic mechanism about Ag/Ni(OH)$_2$ composites was elucidated in Fig. 8c. After the competitive adsorption of the donor BH$_4^-$ and
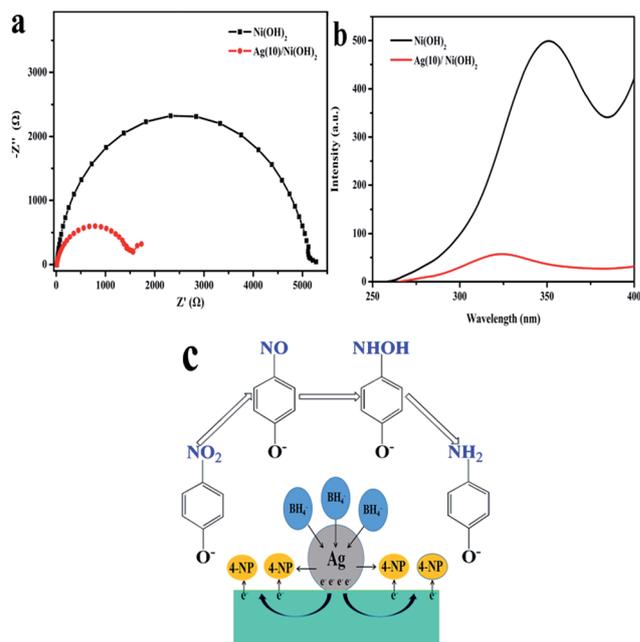

Fig. 8 (a) Nyquist plots for pure Ni(OH)$_2$ and Ag(10)/Ni(OH)$_2$; (b) fluorescence spectra for pure Ni(OH)$_2$ and Ag(10)/Ni(OH)$_2$; (c) possible mechanism for reduction of 4-NP by Ag/Ni(OH)$_2$.

acceptor nitrophenolate onto the surface of Ag/Ni(OH)$_2$ composites, electron transfer takes place between them during the reduction of 4-NP. NaBH$_4$ with high electron injection capability, could contact efficiently with highly dispersed Ag NPs, which act as electron relay in the reaction. Then electrons leave the Ag NPs from the depleted region near the interface of Ag/Ni(OH)$_2$ composite to the Ni(OH)$_2$, and end up with an electron-enriched region according to Fermi level alignment. After that the existence of the surplus electrons added inside the Ni(OH)$_2$ can facilitate the uptake of electrons by 4-NP molecules, which adsorbed on surface of the composites. Thus the nitro group can be reduced to the nitroso group, then turns into hydroxylamine and further reduced to amino group at last.[24,34,35]

4. Conclusions

In summary, a facile autocatalytic reduction method to deposit Ag NPs with an average diameter of around 4.7 nm on Ni(OH)$_2$ nanosheets has been developed. The Ni(OH)$_2$ nanosheets play an important role in the formation of Ag/Ni(OH)$_2$ composites in ethanol at room temperature. The analytic data (UV-visible spectra, TEM, XPS survey) proved the formation of Ag NPs on the surface of Ni(OH)$_2$ nanosheets. The obtained Ag(10)/Ni(OH)$_2$ composites show the highest catalytic activity for reduction of 4-NP by NaBH$_4$. These highly active Ag/Ni(OH)$_2$ composites can be promising materials for supercapacitor and catalyst application.

Acknowledgements

References

1 D. S. Patil, S. A. Pawar, R. S. Devan, M. G. Gang, Y.-R. Ma, J. H. Kim and P. S. Patil, *Electrochim. Acta*, 2013, **105**, 569–577.

2 K. Tedsree, T. Li, S. Jones, C. W. Chan, K. M. Yu, P. A. Bagot, E. A. Marquis, G. D. Smith and S. C. Tsang, *Nat. Nanotechnol.*, 2011, **6**, 302–307.

3 P. Gong, H. Li, X. He, K. Wang, J. Hu, W. Tan, S. Zhang and X. Yang, *Nanotechnology*, 2007, **18**, 10741–10746.

4 Y. Fu, T. Huang, L. Zhang, J. Zhu and X. Wang, *Nanoscale*, 2015, **7**, 13723–13733.

5 H. A. Elazab, S. Moussa, B. F. Gupton and M. S. El-Shall, *J. Nanopart. Res.*, 2014, **16**(7), 1–11.

6 P. Zhang, C. Shao, Z. Zhang, M. Zhang, J. Mu, Z. Guo and Y. Liu, *Nanoscale*, 2011, **3**, 3357–3363.

7 Y. Cai, F. Tan, X. Qiao, W. Wang, J. Chen and X. Qiu, *RSC Adv.*, 2016, **6**, 18407–18412.

8 T. Chen, W. Quan, L. Yu, Y. Hong, C. Song, M. Fan, L. Xiao, W. Gu and W. Shi, *J. Alloys Compd.*, 2016, **686**, 628–634.

9 Y. Zhang, W. Yan, Z. Sun, X. Li and J. Gao, *RSC Adv.*, 2014, **4**(72), 38040–38047.

10 M. Wang, D. Tian, P. Tian and L. Yuan, *Appl. Surf. Sci.*, 2013, **283**, 389–395.

11 Y. I. Seo, K. H. Hong, D. G. Kim and Y. D. Kim, *Colloids Surf., B*, 2010, **81**, 369–373.

12 F. S. Cai, G. Y. Zhang, J. Chen, X. L. Gou, H. K. Liu and S. X. Dou, *Angew. Chem., Int. Ed.*, 2004, **43**, 4212–4216.

13 F. Behnoudnia and H. Dehghani, *Dalton Trans.*, 2014, **43**, 3471–3478.

14 J. Zhong, B. Duan, B. Yan, Y. Feng, K. Zhang, J. Wang, C. Wang, Y. Shiraishi, P. Yang and Y. Du, *RSC Adv.*, 2016, **6**, 72722–72727.

15 L. Pan, L. Li and Y. Chen, *J. Sol–Gel Sci. Technol.*, 2012, **62**, 364–369.

16 J. Zhen, D. Liu, X. Wang, J. Li, F. Wang, Y. Wang and H. Zhang, *Dalton Trans.*, 2015, **44**, 2425–2430.

17 Y. C. Chen, F. C. Zheng, Y. L. Min, T. Wang, Y. X. Wang, Y. G. Zhang, Y. C. Chen, F. C. Zheng, Y. L. Min and T. Wang, *Colloids Surf., A*, 2012, **395**, 125–130.

18 Y.-C. Chen, F.-C. Zheng, Y.-L. Min, T. Wang, Y.-G. Zhang and Y.-X. Wang, *J. Mater. Sci.: Mater. Electron.*, 2012, **23**, 1592–1598.

19 J. Yu, S. Wang, B. Cheng, Z. Lin and F. Huang, *Catal. Sci. Technol.*, 2013, **3**, 1782–1789.

20 C.-E. Shi, L. Pan, C.-R. Wang, Y. He, Y.-F. Wu and S.-S. Xue, *JOM*, 2015, **68**, 324–329.

21 O. Choi, K. K. Deng, N. J. Kim, L. Ross Jr, R. Y. Surampalli and Z. Hu, *Water Res.*, 2008, **42**, 3066–3074.

22 S. Zhang and H. C. Zeng, *Chem. Mater.*, 2009, **21**, 871–883.

23 M. Hu, J. He, M. Yang, X. Hu, C. Yan and Z. Cheng, *RSC Adv.*, 2015, **5**, 26823–26831.

24 Y. Chi, J. Tu, M. Wang, X. Li and Z. Zhao, *J. Colloid Interface Sci.*, 2014, **423**, 54–59.

25 X. Wang, Z. Zhao, D. Ou, B. Tu, D. Cui, X. Wei and M. Cheng, *Appl. Surf. Sci.*, 2016, **385**, 445–452.

26 J. Wang, B. Jin and L. Cheng, *Electrochim. Acta*, 2013, **91**, 152–157.

27 Y. Wang, Y. Li, S. Yang, G. Zhang, D. An, C. Wang, Q. Yang, X. Chen, X. Jing and Y. Wei, *Nanotechnology*, 2006, **17**, 3304–3307.

28 Y.-G. Wu, M. Wen, Q.-S. Wu and H. Fang, *J. Phys. Chem. C*, 2014, **118**, 6307–6313.

29 B. Mu, Q. Wang and A. Wang, *J. Mater. Chem. A*, 2013, **1**(24), 7083–7090.

30 D. Ghosh, S. Giri, A. Mandal and C. K. Das, *Chem. Phys. Lett.*, 2013, **573**, 41–47.

31 Y. Cai, D. Wu, X. Zhu, W. Wang, F. Tan, J. Chen, X. Qiao and X. Qiu, *Ceram. Int.*, 2017, **43**, 1066–1072.

32 H. Yan and H. Yang, *J. Alloys Compd.*, 2011, **509**, L26–L29.

33 J. Wang, Z. Wang and Z. Zhu, *Appl. Catal., B*, 2017, **204**, 577–583.

34 Z. Jiang, D. Jiang, W. Wei, Z. Yan and J. Xie, *J. Mater. Chem. A*, 2015, **3**, 23607–23620.

35 Z. Jiang, X. Lv, D. Jiang, J. Xie and D. Mao, *J. Mater. Chem. A*, 2013, **1**, 14963–14972.